이학석사 학위논문

마우스 피부 이식모델의 갈색 지방에서의 면역반응과 세라마이드대사

The immune responses in the brown fat and ceramide metabolism in a mouse skin graft model

울 산 대 학 교 대 학 원

의 학 과

TRAN HUU PHUC

마우스 피부 이식모델의 갈색 지방에서의 면역반응과 세라마이드대사

지 도 교 수　　황 신

이 논문을 이학석사학위 논문으로 제출함

2020 년 08 월

울 산 대 학 교 대 학 원

의　　학　　과

쩐 후 푹

쩐 후 푹의 이학석사학위 논문을 인준함

심사위원 정 동 환 (인)

심사위원 황 신 (인)

심사위원 김 나 영 (인)

울 산 대 학 교 대 학 원

2020년 08월

Master of Science

The immune responses in the brown fat and ceramide metabolism in a mouse skin graft model

The Graduate School

of the University of Ulsan

Department of Medicine

Tran Huu Phuc

The immune responses and ceramide metabolism in a mouse skin graft model

Supervisor: Prof. Shin Hwang

A Dissertation

Submitted to

The Graduate School of the University of Ulsan

In Partial Fulfillment of the Requirements

For the Degree of

Master of Science

by

Tran Huu Phuc

Department of Medicine

Ulsan, Korea

August, 2020

Contents

요약 iii

Introduction 1

Materials & Methods 7

Murine skin graft model 7

Histology 8

Brown fat immune cell isolation 8

Flow cytometry 9

RNA isolation and quantitative reverse transcription PCR 10

Statistical analysis 14

Result 15

Reduced BF in allogeneic skin graft mice 15

Characterization of T cells in the BF 18

The expression of CD36 and CD69 on T cells 22

Characterization of DCs in the BF 25

The expression of MHC II, CD86 and CD36 in DCs 28

The expression of MHC II, CD86 and CD36 in monocytes/macrophages 32

The expression of inflammatory monocytes in the BF in a skin graft model 36

The expression of the enzymes in ceramide metabolism upon acute rejection 39

Discussion 42

References 49

Abstract 63

그림목차

Table 1. Primer list for Q-PCR 12

Figure 1. The histology, weight and cell numbers of the BF 17

Figure 2. T cells and their subsets in the BF 21

Figure 3. The expression of CD69 and CD36 in T cells 23

Figure 4. DC subsets in BF and drLNs 26

Figure 5. The expression of MHC II, CD86 and CD36 in DC 31

Figure 6. The expression of MHC II, CD86 and CD36 in monocytes/ macrophages cells 35

Figure 7. The expression of inflammatory monocytes in the BF in a skin graft model 38

Figure 8. The expression of the enzymes in ceramide metabolism in the livers from skin graft mice 41

요약

배경 : 이식 거부반응은 T 림프구가 중요한 역할을 하는 동종 이식의 주요 단점이다. 지질 대사는 지방 조직이 면역계와 밀접하게 연결되어있는 동안 T 림프구의 적절한 분화 및 기능에 기여한다. 그러나 지방 조직 면역 세포의 특성 및 역할은 이식 거부반응에서 연구된 바가 없다.

목적 : 이 연구는 쥐 피부 이식 모델에서 갈색 지방의 면역 반응을 설명하기 위해 수행된다. 이 연구는 또한 거부 반응에서 세라마이드 대사의 역할을 이해하는데 도움이 될 수 있다.

방법 : 동종 마우스 꼬리 피부를 사용하여 수령자 마우스의 좌측 상부 후면에서 피부 이식편을 수행하였다. 3 일 또는 7 일 후에 마우스를 희생시키고 액체 질소에서 즉시 냉동시킨 다음 Q-PCR을 사용하여 세라마이드 효소의 발현을 평가할 때까지 -80 ℃에서 보관하였다. 또는 조직학검사를 위해 지방 조직을 포르말린에 고정시켰다. 갈색 지방 및 배수 림프절을 단일 세포로 분리하고 유세포 분석에 사용하여 T 림프구 및 항원-제시 세포의 아형을 분석하였다.

결과 : 피부 동종 이식 7일 후 동종 이형 피부 이식 마우스 갈색 지방 (BF)의 무게가 유의하게 감소한 것을 발견했지만, 면역 세포 수에는 차이가 없었다. 유세포 분석의 결과는 BF의 $CD8^+$ T 세포 및 $CD36^+$ 수지상 세포 (DC)가 7 일 후에 동종 이형 피부 이식편에 의해 증가되었지만 항원제시 세포 (APC)의 분포에는 변화가 없음을 보여준다. CerS5 및 Smpd1의 발현은 7 일차에 이식 거부반응에 의해 간에서 증가하였다.

결론 : BF의 $CD8^+$ T 세포와 $CD36^+$ DC는 피부 이식편의 급성 거부에 기여할 수 있다. 또한 세라마이드 대사도 이식거부반응에 의해 변화하였고, 이는 이식거부반응이 지방조직과 지질대사에 영향을 줄 수 있음을 시사한다.

Introduction

The allogeneic graft is the transplantation of an organ or tissue from one individual to another of the same species with a different genotype. The use of allotransplantation tissues has many clinical advantages. Allogeneic tissue would be similar in composition and, depending upon the specific tissue and application, may contain relevant signaling cues to facilitate the healing process and integrate the donor tissue into the recipient [1]. According to Korean Organ Transplantation Registry (KOTRY), there is a higher increment in deceased donor organ for allotransplantation, from 233 cases in 2000 to 1989 cases in 2015, in parallel with the increment of deceased donors from 1.09 per million population in 2000 to 9.72 per million population in 2015 [2].

One major drawback to allogeneic transplantation is the need for continuous, indefinite immunosuppression to prevent acute graft rejection [3]. Rejection of solid organ allogeneic grafts is the result of a complex series of interactions involving coordination between both the innate and adaptive immune systems with T cells which are central to this process [4].

Allospecific T cells become activated through the interaction of their T cell receptors with intact allogeneic major histocompatibility complex (MHC) molecules on donor cells (direct pathway) and/or donor peptides presented by self-MHC molecules on recipient antigen-presenting cells (APCs) such as macrophages or dendritic cell (indirect pathway) [5]. Once recipient T cells become activated, they undergo clonal expansion, differentiate into effector cells, and migrate into the graft, resulting in promoting tissue destruction [4]. In a skin graft model, for example, $CD4^+$ T cells facilitate $CD8^+$ T cell differentiation into cytotoxic T cells (CTLs) either by cell-to-cell contact or by secretion of IL-2/IFN-γ cytokines [6]. CTLs accumulate surrounding the graft and secrete perforin and granzyme B, or induce the Fas/FasL pathway, which induces target cell apoptosis [6]. To solve this setback in allotransplantation, researchers have focused on manipulating the immune response to create a state of tolerance in immunity [7-9].

Upon antigen recognition and co-stimulation, T lymphocytes upregulate the metabolic machinery necessary to proliferate and sustain effector function [10]. Thus, strategies designed to inhibit metabolic reprogramming from preventing naive T cells from activating

and differentiating into effector T cells might provide a means to inhibit transplant rejection [10]. For example, blocking glycolysis by 2-deoxy-D-glucose and rapamycin inhibits effector development but promotes regulatory T cells (Tregs) formation [11]. Alternatively, Tregs are not dependent upon glycolysis and appear to rely more on lipid oxidation to generate energy [12, 13]. Amongst immune metabolism, lipid metabolism is central to the appropriate differentiation and functions of T lymphocytes, and ultimately to the maintenance of immune tolerance [14]. Activated T cells can increase the decomposition of glutamine and reduce fatty acid oxidation to meet the requirement of energy, cell growth, proliferation, differentiation, and cytokine secretion [15]. Sullivan, et al. demonstrate that effector T cells can obtain fatty acids for the microenvironment, while memory T cells only use carbon derived from glucose metabolism to synthesize fatty acids [16]. Similarly, lipid metabolism is proved as important for maintaining the balance between effector T cells and Tregs [17]. Much of the work has focused on the role of metabolism in facilitating or controlling immune cell differentiation and determination of effector mechanisms to understand to what extent the coordination of metabolism impacts on immunity and immune

tolerance [7].

Ceramide is a central molecule of sphingolipid metabolism, which is involved in numerous cellular processes, ranging from proliferation and differentiation of the cells to inflammatory responses and cellular apoptosis as well as regulates lipid metabolism [18, 19]. Ceramide, produced through either the induction of sphingomyelin hydrolysis or synthesized *de novo,* transduces signals mediating differentiation, growth, growth arrest, apoptosis, cytokine biosynthesis, secretion, and a variety of other cellular functions [20]. The ceramide-metabolizing enzyme, acid sphingomyelinase, has been shown to play a key role in the degranulation of T cells, a mechanism critical to their effector function [21]. Besides macrophages and T cells, ceramide may drive activation of other types of immune cells. For example, ceramide/sphingomyelinases are reported to mediate natural killer cell signals [22]. Meanwhile, more evidence has indicated that, in response to TCR/CD3 engagement and other stimulations, sphingomyelinases become activated to generate ceramide, which further mediates downstream signals and subsequent T-cell activation [23, 24]. Nonetheless, the role of ceramide is mainly as an indicator of the inflammatory response, while its function in

allogeneic transplantation has not been elucidated yet [25].

Adipose tissues (AT) are closely connected with the immune system. The adipose tissues secreting a series of immune regulators called adipokines, represent the common mediator linking metabolic processes and immune functions [26]. Adipose tissue is a complex immunocompetent organ, enriched with adipocytes and immune cells that contribute to metabolic, endocrine, and immune activities [27]. While the brown adipose tissues (BAT or BF), are associated with energy expenditure and thermogenesis specifically in infants and hibernating animals, the white adipose tissues (WAT or WF) are the energy storage depot for excess nutrients in the form of lipids that serves as a sensor for the energy balance of the body [26, 28]. WF is localized in different sites of the body and can be found under the skin as subcutaneous adipose tissue (SAT) and in the abdominal cavity as visceral adipose tissue (VAT) [26]. Adipose tissue has remained a largely unexplored and unappreciated immune site and only recently emerged that it harbors a unique profile of immune cells, with either pro-inflammatory (M1 macrophages, dendritic and mast cells, neutrophils, Th1, $CD4^+$ and $CD8^+$ T cells, B lymphocytes) or anti-inflammatory (M2

macrophages, eosinophils, Tregs and Th2 $CD4^+$ T cells) activity, playing a pivotal role in immune homeostasis and metabolic regulation of AT [27]. However, research on the function of adipose tissue and lipid bodies, especially in the BF in transplantation has not been conducted yet.

Our previous observation showed that the sizes of BF located in the back appeared to be reduced in the mice subjected to an allogeneic skin graft, while the sizes and cell numbers of draining lymph nodes (drLNs) increased as expected. Therefore, I investigated the contents of lipid metabolism and immune cells using a grafted skin model. Through flow cytometry and Q-PCR, I elucidated which immune cells in the BF were involved in allogeneic immune responses in skin graft and whether ceramide metabolism was changed in acute rejection in mice.

Materials & Methods

Murine skin graft model

The murine skin graft was performed following standard protocols with minor modifications [29]. Sex-and age-matched BALB/C as the recipient and C57BL/6 mice as allogeneic donor were used (OrientBio, Gyeonggi-do, Korea). Recipients were given C57BL/6 mice tail skin as the graft tissue. Recipient mice were anesthetized with Zoletil 50 (Virbac, Seoul, South Korea) and Rompun (Bayer Korea, Seoul, South Korea) and shaved around the flank. A graft bed on the left lateral thorax was prepared with fine scissors by removing an area of the epidermis. Skins for grafts 0.8 – 1 cm^2 in an area were fitted to the prepared bed with suturing and then covered with Mepitel One (Mölnlycke Health Care, Belrose, Australia), gauze and surgical tape. Mice were sacrificed after 3 or 7 days and tissues were immediately frozen in liquid nitrogen and then stored at -80 ˚C until use or isolated for Q-PCR. Alternatively, tissues were fixed in Formalin or single cell suspension was made for flow cytometry. All the procedures were approved by IACUC, AMC (Approval No. 2019-12-345).

Histology

Whole fat tissue was fixed in 4% formalin, embedded in paraffin, sectioned, and stained with hematoxylin-eosin (H&E) following standard protocols. The preparation of the slides was performed by Comparative Pathology Core Facility, Convergence Medicine Research Center, Asan Medical Center. The magnification was x40 and x200.

Brown fat immune cell isolation

Brown fat tissue was chopped up with scissors and dissociated using GentleMACS dissociator (Miltenyi Biotec, Bergisch Gladbach, Germany) in dissociation buffer (0.5M bovine serum albumin (BSA; Bovogen, Australia), 2 mg/ml Collagenase Type II (Sigma Aldrich, St. Louis, MO) in Hank's 1X Balanced Salt Solutions (HBSS; Hyclone, Logan, Utah). The tissue was incubated in incubator 37^0C on 30 minutes before being homogenized by a syringe plunger and filtered with a 100 μm nylon cell strainer (CORNING, Corning, NY) then washed twice with 1x PBS. Cells were suspended in Dulbeco's modified Eagle's medium (DMEM; Hyclone, Logan, UT, USA) supplemented with 10% fetal bovine serum (FBS) (Sigma-Aldrich, St. Louis, MO, USA), 100 U/mL penicillin and 100 μg/mL

streptomycin (Corning, Manassas, VA, USA),.and the cell number was counted using a hemocytometer for further experiment.

For immune cell isolation from drLNs, the tissue was homogenized with a syringe plunger in 5 mL RPMI 1640 (Welgene, Gyeongsan-si, Gyeongsangbuk-do, Republic of Korea) and filtered with a 100 μm nylon cell strainer (CORNING, Corning, NY) then washed twice with 1x PBS. Cells were suspended in RPMI 1640 (Welgene, Gyeongsan-si, Gyeongsangbuk-do, Republic of Korea) with 10% FBS (Sigma Aldrich, St. Louis, MO), 55 μM 2- Mercaptoethanol (Gibco, Waltham, MA) 1 mM sodium pyruvate (Sigma Aldrich, St. Louis, MO), 1% Penicillin/streptomycin (CORNING, Corning, NY), and the cell number was counted using a hemocytometer for further experiment.

Flow cytometry

Isolated immune cells as above were prepared at $1x10^6$ cells/tube for surface staining. Cells were treated with Fc-blocking rat anti-mouse CD16/32 monoclonal antibody (mAb) (clone 2.4G2, BioLegend) to prevent nonspecific binding, and stained with fluorescence-conjugated anti-CD11b (clone M1/70, BioLegend), anti-CD45 (clone 30-F11,

BD), anti-CD11c (clone N418, BioLegend), anti-MHC class II (clone M5/114.15.2, BioLegend), anti-CD86 (clone GL-1, BioLegend), anti-B220 (clone RA3-6B2, BioLegend), anti-CD3 (clone 145-2C11, eBiosciences), anti-CD4 (clone RM4-5, eBiosciences), anti-CD8 (clone 53-6.7, BioLegend), , anti-CD44 (clone G44-26, BD), anti-CD62L (clone MEL-14,BD), anti-CD69 (clone H1.2F3, BioLegend) , anti-CD36 (clone HM36, BioLegend) and anti-Ly6C (clone HK1.4, BioLegend) monoclonal antibodies (mAbs) at 4℃ for 30 minutes. Flow Cytometric analysis was performed with a CytoFlex flow cytometer (Beckman Coulter, Brea, CA) and analyzed with a FlowJo V10 software (FlowJo, LLC., Ashland, OR). Absolute cell numbers for each subpopulation were calculated by multiplying the percentage of each population by the weight of the BF.

RNA isolation and quantitative reverse transcription PCR

Total RNA was extracted from the liver tissue using the TRIzol reagent (Invitrogen, Carlsbad, CA), and the concentration and purity of RNA were measured using Nanodrop 2000 (Thermo Fisher Scientific, Waltham, MA). Total RNA of 0.5 μg for BF and drLNs or 5 μg for other tissues was used to synthesize cDNA using Oligo(dT)12-18 primer, SuperScript

III Reverse Transcriptase, 10 mM dNTP Mix, and RNase OUT (all from Invitrogen, Carlsbad, CA). Messenger RNA (mRNA) expression for ceramide enzymes was quantified by SYBR Green (Applied Biosystems, Foster City, CA) two-step real-time RT-PCR, using an ABI 7900 Sequence Detection System (Applied Biosystems, Foster City, CA). Mouse primer sequences are shown in table 1. All reactions were performed in triplicates using thermal cycling conditions as follow; 2 minutes at 50℃, 10 minutes at 95℃ followed by 40 cycles of 95℃, 15 seconds, and 60℃, 1 minute. Ct value was determined by an SDS software v2.4 (Applied Biosystems, Foster City, CA). The expression of each gene was normalized to Gapdh and Hprt mRNA content and calculated using comparative Ct methods [30].

Table 1. Primer list for Q-PCR

	Gene name	Primer name	Sequence	Reference
1	Gapdh	Forward	TTG TCA GCA ATG CAT CCT GCA C	[31]
		Reverse	ACA GCT TTC CAG AGG GGC CAT C	
2	Hprt	Forward	TGC CGA GGA TTT GGA AAA AGT G	[32]
		Reverse	AGA GGG CCA CAA TGT GAT GG	
3	Ceramide synthase 1 (CerS1)	Forward	GCC ACC ACA CAC ATC TTT CGG	[33]
		Reverse	GGA GCA GGT AAG CGC AGT AG	
4	Ceramide synthase 2 (CerS2)	Forward	AGA GTG GGC TCT CTG GAC G	[33]
		Reverse	CCA GGG TTT ATC CAC AGT GAC	
5	Ceramide synthase 3 (CerS3)	Forward	CCT GGC TGC TAT TAG TCT GAT G	[33]
		Reverse	CTG CTT CCA TCC AGC ATA GG	
6	Ceramide synthase 4 (CerS4)	Forward	GAC CGT GAT GGC CTG GTG TT	[34]
		Reverse	TCT CCT GAT TGG ATC CTG CA	
7	Ceramide synthase 5 (CerS5)	Forward	TGG CCA ATT ATG CCA GAC GTG AG	[33]
		Reverse	GGT AGG GCC CAA TAA TCT CCC AGC	
8	Ceramide synthase 6 (CerS6)	Forward	GCA TTC AAC GCT GGT TTC GAC	[33]
		Reverse	TTC AAG AAC CGG BAC TCC GTA G	

9	Sphingomyelin synthase 1 (Sgms1)	Forward	CCT AAG TGT CTG CAT GGG AGT TGA	[35]
		Reverse	TTT GAT ACA CCG TCT CTG CTG ACT G	
10	Sphingomyelin synthase 2 (Sgms2)	Forward	TCT TCA GCG GCC ACA CTG TC	[35]
		Reverse	AGA TGA TCC CAG CCG CAC TC	
11	Sphingomyelin Phosphodiesterase 1 (Smpd1)	Forward	CAG TTC TTT GGC CAC ACT CA	[36]
		Reverse	CGG CTC AGA GTT TCC TCA TC	
12	Sphingomyelin Phosphodiesterase 3 (Smpd3)	Forward	AGA GCA GGG CTG ACT CCA	[37]
		Reverse	TGG CTC TAG TCA CAC GTT GG	
13	Acid ceramidase (Asah1)	Forward	AAT AAC ACT TGG GTT GTC AC	[38]
		Reverse	TAG GAT ACC CAG ATA ACC AC	
14	Neutral ceramidase (Asah2)	Forward	GAC CCA TCA GAC CTT CCT CA	[38]
		Reverse	CCC TTG TGC CAA TAA AAA CG	
15	Alkaline ceramidase 2 (Acer2)	Forward	GTG TGG CAT ATT CTC ATC TG	[39]
		Reverse	TAA GGG ACA CCA ATA AAA GC	
16	Alkaline ceramidase 3 (Acer3)	Forward	GAT TCA CTG AGG AAC TTT CG	[38]
		Reverse	AGA GAA ACT TCA CTT TTG GC	

Statistical analysis

Student *t*-test and standard error of the Mean (SEM) were calculated by MS EXCEL (Microsoft Corporation, Redmond, WA), *P<0.05; **P<0.01; ***P<0.001.

Result

Reduced BF in allogeneic skin graft mice

I set up the experiment to investigate the roles of immune cells in the BF in a murine allogeneic skin graft model by histology and cell counting. As shown in Fig. 1A, the mononuclear cells (blue dots) appeared slightly more abundant in the BF from allogeneic skin graft mice than those in syngeneic ones, and it is also seen in the WF. The weight of the BF decreased significantly by 20% in allogeneic skin graft mice after 7 days, compared with syngeneic ones (Fig. 1B). There was no change at Day 3. On the other hand, the actual mononuclear cell numbers in the BF did not change between syngeneic and allogeneic graft mice (Fig. 1C).

Figure 1.

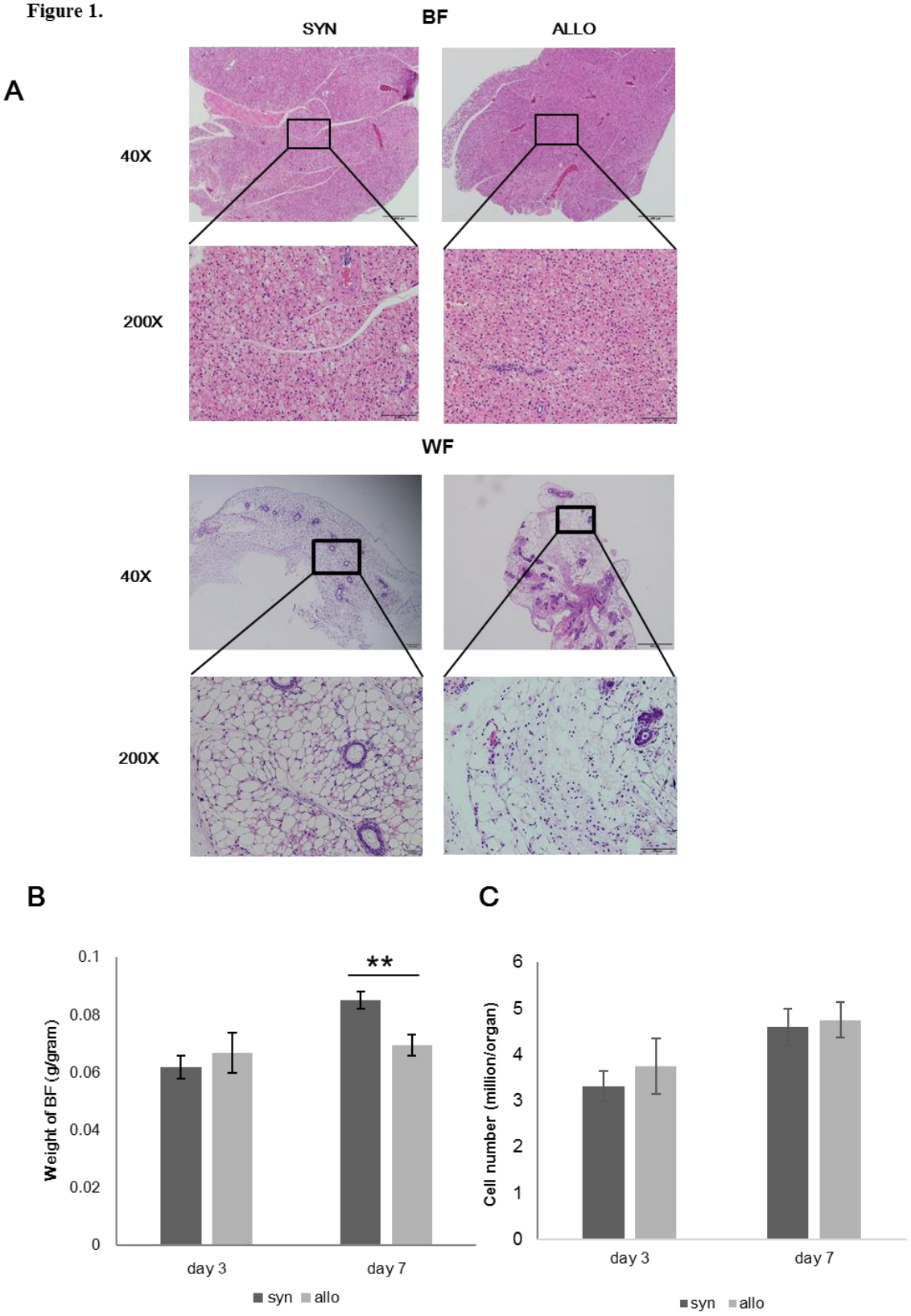
A
SYN
BF
ALLO
40X
200X
WF
40X
200X
B
C
Weight of BF (g/gram)
0.1
0.08
0.06
0.04
0.02
0
**
day 3
day 7
syn
allo
Cell number (million/organ)
6
5
4
3
2
1
0
day 3
day 7
syn
allo

Figure 1. The histology, weight and cell numbers of the BF

(A) Representative histological results show H&E-stained BF (upper) and WF (lower) sections from syngeneic and allogeneic skin graft mice after 7 days. The inset boxes are further magnified to x200 in the lower row. (B) The graph indicates the weight changes of BF after skin transplantation; N = 8 for Day 3 and N = 18 for Day 7 (C) The number of the mononuclear cells in the BF were calculated from flow cytometric results in Fig.2. N = 8 for Day 3 and N = 14 for Day 7. Syn: syngeneic; Allo: allogeneic.

Characterization of T cells in the BF

T cells and their subsets were characterized in the BF from syngeneic and allogeneic skin graft mice by flow cytometry. Cells were isolated from BF at Day 3 or Day 7 post skin graft. The gating strategy was seen in Fig. 2A. Although the drLNs in Day 7 were enlarged visibly in allogeneic skin graft mice (data not shown), T cell numbers were decreased 10% in the drLNs at Day 7 (Fig. 2C). The percentages and the absolute numbers of $CD8^+$ T cells at Day 7 were approximately 1.6 folds, higher in the drLNs from allogeneic skin graft mice than their syngeneic counterparts (Fig. 2C, 2D). There were no differences in $CD4^+$ T cell subsets in BF from allogeneic skin graft mice. In addition, the expression of Te, Tm and Tn in both $CD4^+$ T cells and $CD8^+$ T cells from the BF and drLNs were not different between syngeneic and allogeneic skin graft mice. Noticeably, nearly 35% of total T cells in the BF remained $CD4^-CD8^-$ which could be NK T cells or γδ T cells.

Figure 2.

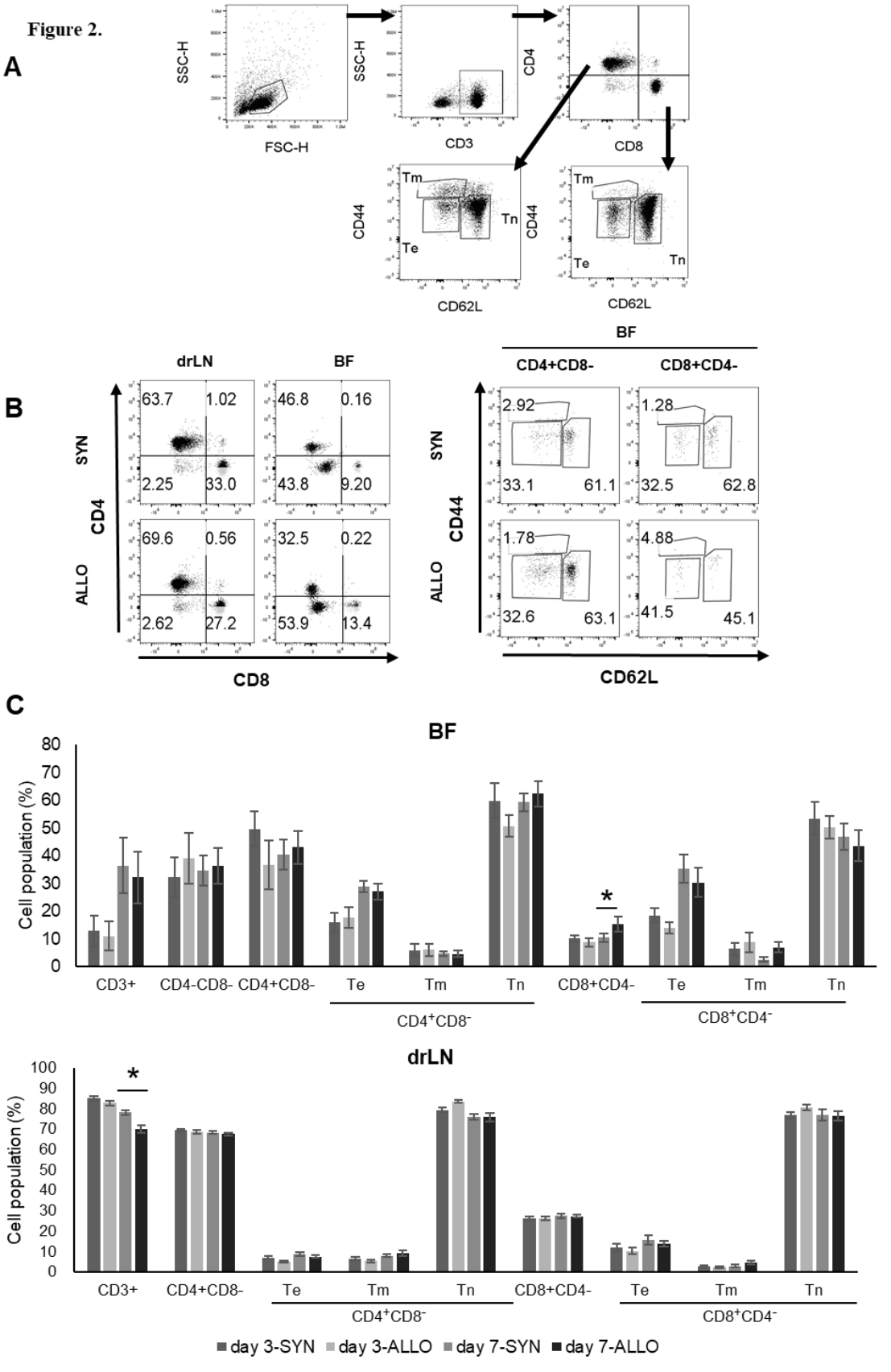
A
SSC-H
FSC-H
SSC-H
CD3
CD4
CD8
CD44
CD62L
Tm
Tn
Te
B
drLN
BF
CD4+CD8-
CD8+CD4-
SYN
ALLO
CD4
CD44
CD8
CD62L
63.7
1.02
2.25
33.0
46.8
0.16
43.8
9.20
69.6
0.56
2.62
27.2
32.5
0.22
53.9
13.4
2.92
33.1
61.1
1.28
32.5
62.8
1.78
32.6
63.1
4.88
41.5
45.1
C
BF
drLN
Cell population (%)
CD3+
CD4-CD8-
CD4+CD8-
CD8+CD4-
Te
Tm
Tn
CD4+CD8-
CD8+CD4-
*
day 3-SYN
day 3-ALLO
day 7-SYN
day 7-ALLO

Figure 2. (continued)

D

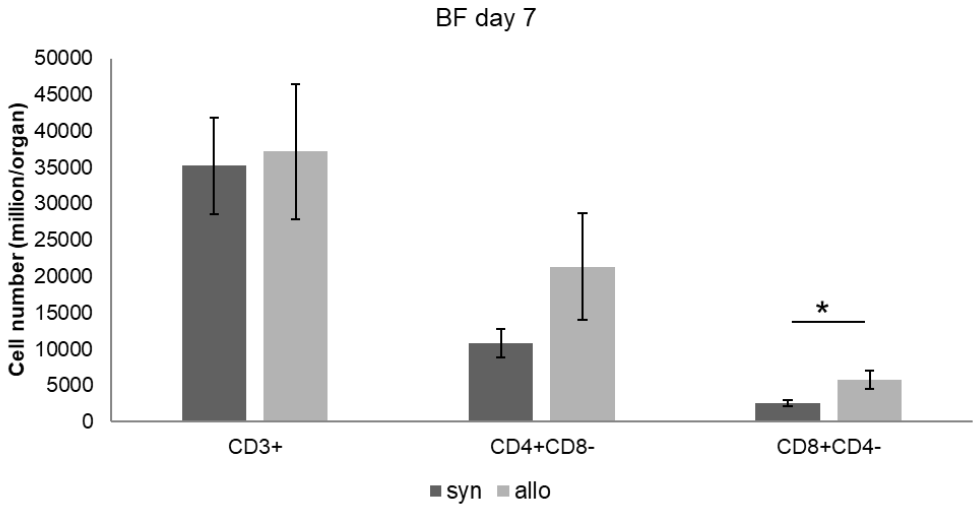

Figure 2. T cells and their subsets in the BF

Immune cells in the BF and drLNs were isolated from syngeneic and allogeneic skin graft mice at Day 3 and Day 7. Flow cytometry was performed to evaluate T cell subsets. (A) Live cells were gated by SSC/FSC, and T cells were defined as $CD3^+$ cells. $CD4^+$ and $CD8^+$ T cells were analyzed in $CD3^+$ T cells as $CD4^+CD8^-$ and $CD8^+CD4^-$. $CD4^+$ and $CD8^+$ T cells were divided into three subsets, which were defined as $CD44^{lo}CD62L^{lo}$ effector T cell (Te), $CD44^{hi}CD62L^{lo}$ memory T cells (Tm) and $CD44^{lo}CD62L^{high}$ naïve T cells (Tn) [40]. (B) Representative flow cytometric plots show T lymphocytes in the BF and drLNs (left) and their subsets (right). (C) The graphs present the percentages of T cell subsets in the BF and drLNs. (D) The absolute numbers of T cells in the BF were calculated per organ. N = 8 for Day 3 and N = 14 for Day 7.

The expression of CD36 and CD69 on T cells

The expression of CD36, fatty acid translocase, and CD69, a lymphocyte activation marker, was assessed. The gating strategy was shown in Fig. 3A. There were no remarkable changes in the expression of CD69 among groups. CD36 in $CD4^+$ T cells from allogeneic skin graft mice was expressed higher, compared with those of syngeneic ones in BF at Day 7 ($p=0.06$) (Fig. 3B, C).

Figure 3.

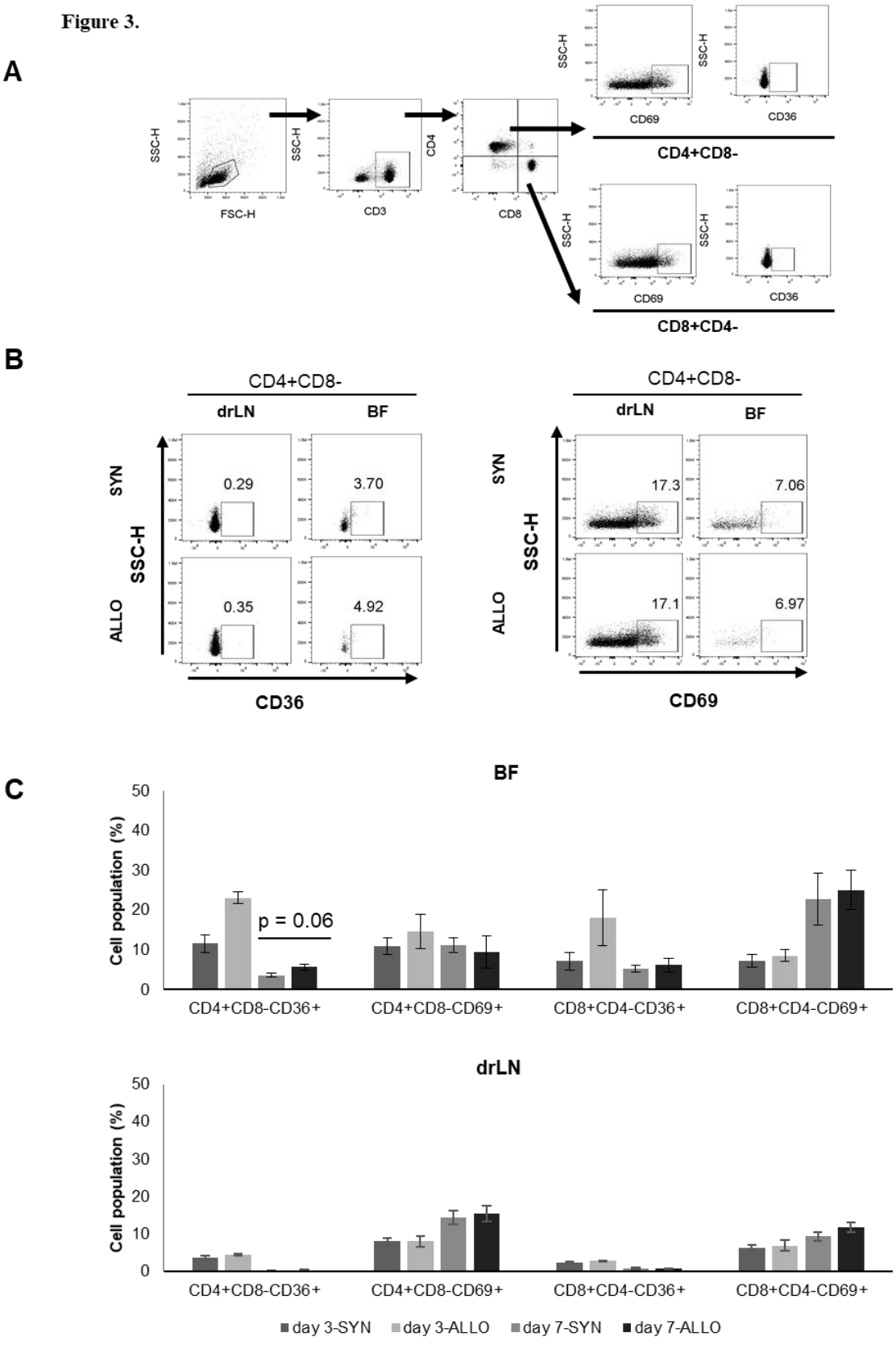
A
SSC-H
FSC-H
CD3
CD4
CD8
CD69
CD36
CD4+CD8-
CD8+CD4-
B
CD4+CD8-
drLN
BF
SYN
ALLO
SSC-H
0.29
3.70
0.35
4.92
17.3
7.06
17.1
6.97
CD36
CD69
C
BF
drLN
Cell population (%)
p = 0.06
CD4+CD8-CD36+
CD4+CD8-CD69+
CD8+CD4-CD36+
CD8+CD4-CD69+
day 3-SYN
day 3-ALLO
day 7-SYN
day 7-ALLO

Figure 3. The expression of CD69 and CD36 in T cells

(A) Live cells were gated by SSC/FSC and T cells were defined as $CD3^+$. $CD4^+$ and $CD8^+$ T cells were analyzed in $CD3^+$ T cells as $CD4^+CD8^-$ and $CD8^+CD4^-$. $CD69^+$ and $CD36^+$ cells were analyzed in $CD4^+CD8^-$ and $CD8^+CD4^-$ cells. (B) Representative flow cytometric plots show CD36 and CD69 expression from $CD4^+CD8^-$ subsets in the BF and drLNs. (C) The graphs present the expression of CD36 and CD69 in the BF and drLNs. N = 8 for Day 3 and N = 14 for Day 7.

Characterization of DCs in the BF

Myeloid cells, such as DCs (Fig. 4) and monocytes/macrophages (Fig. 5), were characterized in the BF. DCs contained two subsets: cDCs and pDCs, which were defined respectively as $CD11c^{+}B220^{-}$ and $CD11c^{+}B220^{+}$. The subsets of cDCs and pDCs were distinguished by Ly6C and MHC II expression, as shown in Fig. 4A. Functionally, cDC1 has a superior ability to present antigens to $CD8^{+}$ T cells, whereas cDC2 has a predominant role in antigen presentation to $CD4^{+}$ T cells [41]. pDCs are shown to contribute to inflammatory responses in the steady state and pathology, and to the proinflammatory activation of cytotoxic T cells and cDCs [42]. Although total $CD45^{+}$ cells were increased from Day 3 to Day 7, all the subsets of DC in BF did not change between syngeneic and allogeneic ones (Fig. 4B, C). The cDC2 and pDC2 subsets were increased twice in the drLNs allogeneic skin graft mice than those in the syngeneic counterpart. The increase was statistically significant (Fig. 4C).

Figure 4.

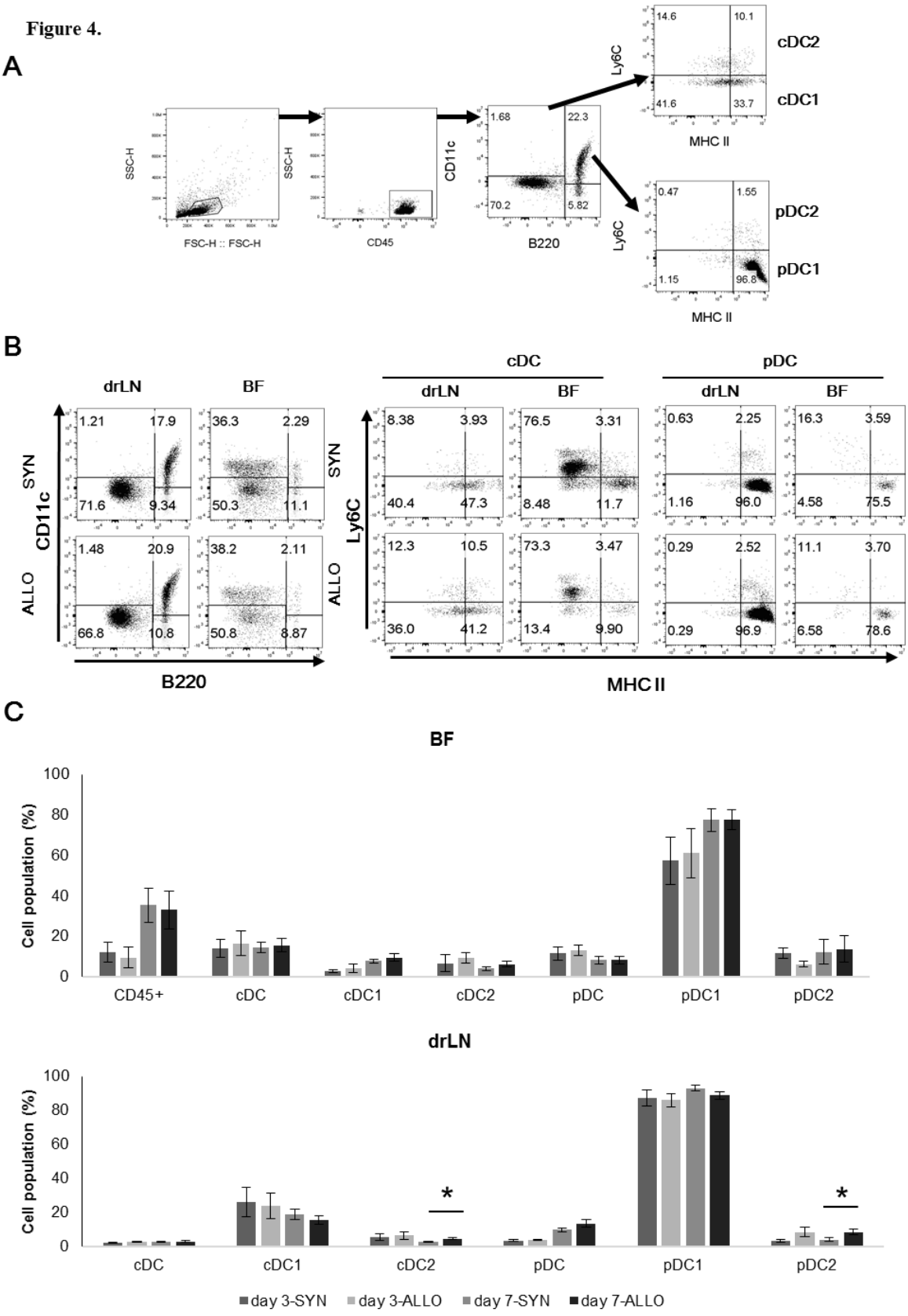
A
SSC-H
FSC-H :: FSC-H
CD45
CD11c
B220
Ly6C
MHC II
cDC2
cDC1
pDC2
pDC1
B
drLN
BF
cDC
pDC
SYN
ALLO
CD11c
B220
Ly6C
MHC II
C
BF
drLN
Cell population (%)
CD45+
cDC
cDC1
cDC2
pDC
pDC1
pDC2
day 3-SYN
day 3-ALLO
day 7-SYN
day 7-ALLO

Figure 4. DC subsets in BF and drLNs

(A) Live cells were gated by SSC/FSC and immune cells were defined as $CD45^+$. Dendritic cells were divided into two subsets, which were defined as $CD11c^+B220^+$ plasmacytoid dendritic cells (pDCs) and $CD11c^+B220^-$ conventional dendritic cells (cDCs). (B) Representative flow cytometric plots show pDCs, cDCs, and their type 1 and 2 subsets in the BF and drLNs. (C) The graphs indicate the percentages of DC subsets in the BF and drLNs; N = 8 for Day 3 and N = 14 for Day 7.

The expression of MHC II, CD86 and CD36 in DCs

I next evaluated DC activation by assessing MHC II and CD86 expression as well as the expression of CD36 in DCs. The gating strategy was seen in Fig. 5A. The percentages of $CD11c^+$ DC population were significantly increased in the drLNs by 1.3 folds in allogeneic skin graft mice but remained unchanged in the BF in all groups (Fig. 5C). Similarly, there were no significant differences in the expression of the activation markers on DC in the drLNs and BF. CD36 was expressed higher in DCs in the BF than that of the drLNs and $CD36^+CD11c^+$ cells were increased about 1.5 folds in allograft mice, compared with those of syngeneic ones. The increase was statistically significant (Fig. 5C).

Figure 5.

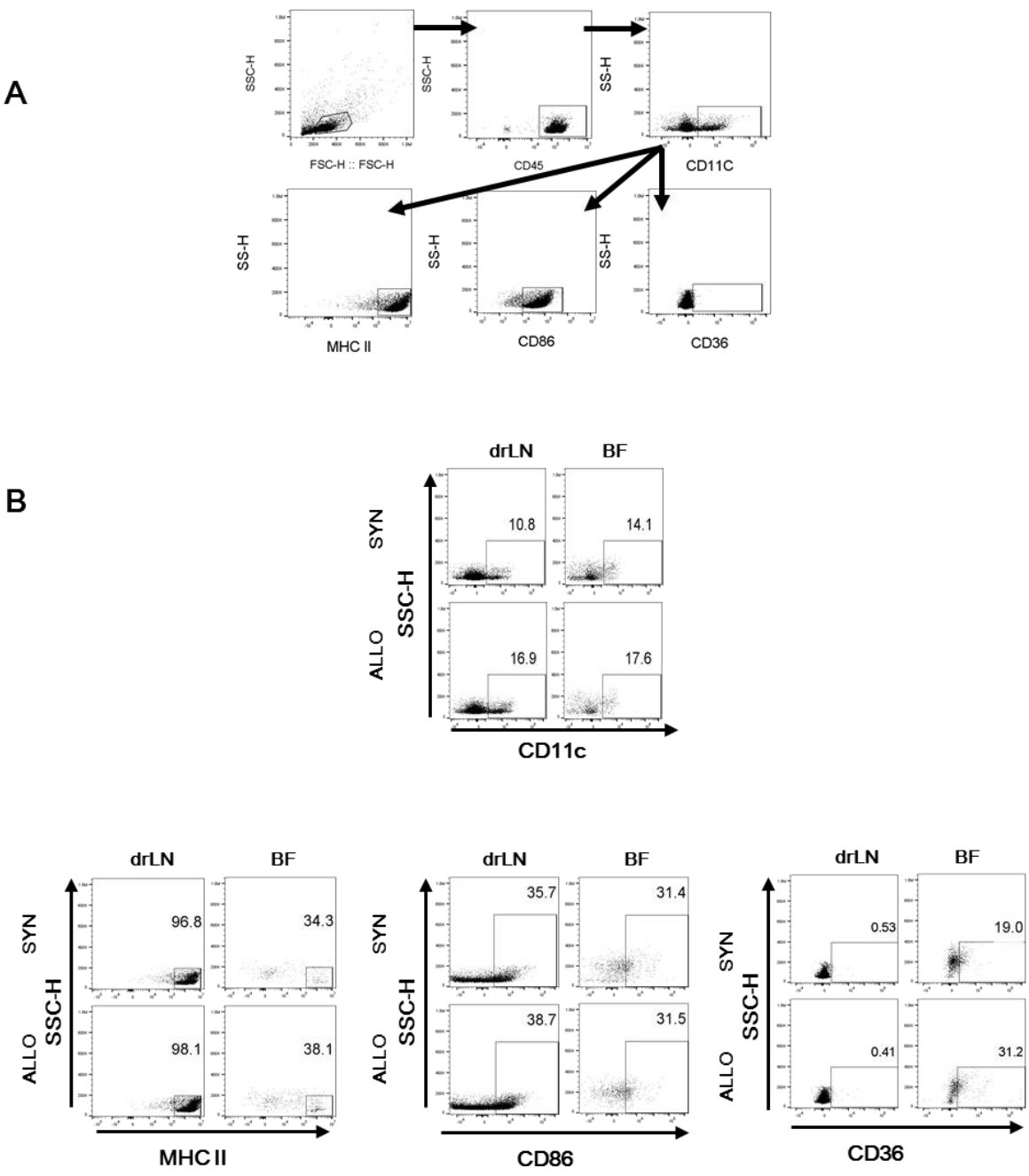
A
SSC-H
FSC-H :: FSC-H
SSC-H
CD45
SS-H
CD11C
SS-H
MHC II
SS-H
CD86
SS-H
CD36
B
drLN
BF
SYN
SSC-H
ALLO
10.8
14.1
16.9
17.6
CD11c
drLN
BF
96.8
34.3
98.1
38.1
MHC II
drLN
BF
35.7
31.4
38.7
31.5
CD86
drLN
BF
0.53
19.0
0.41
31.2
CD36

Figure 5. (continued)

C

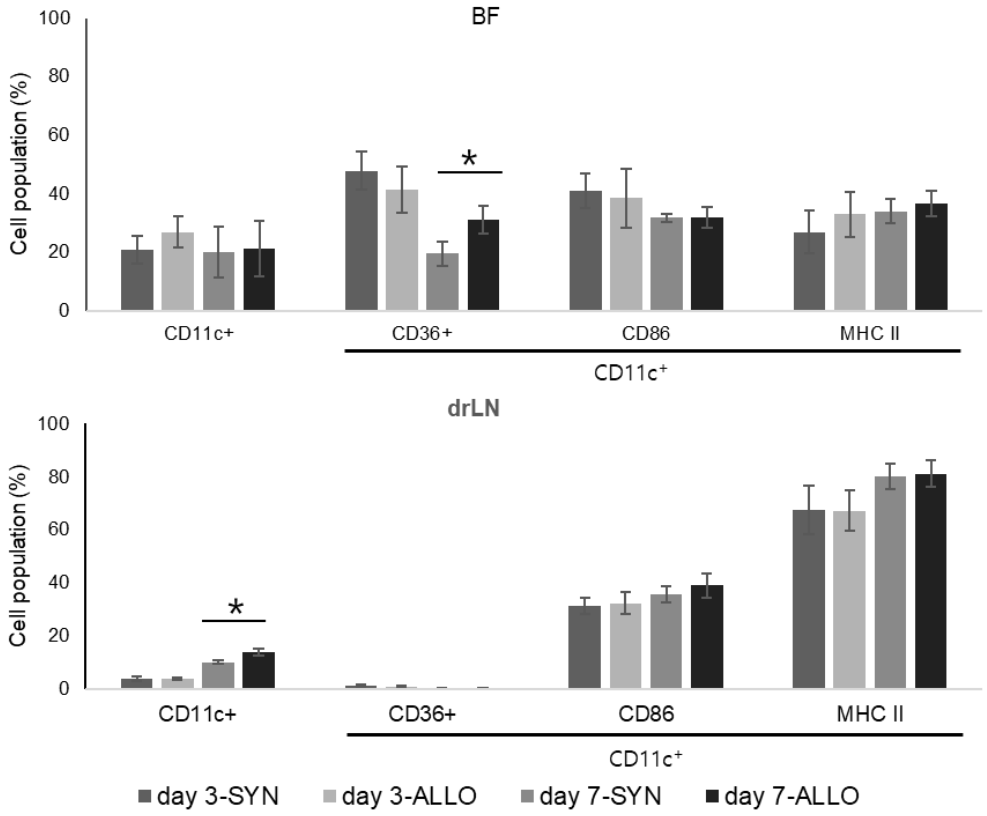

Figure 5. The expression of MHC II, CD86 and CD36 in DC

(A) Live cells were gated by SSC/FSC and immune cells were defined as $CD45^+$. DCs were defined as $CD45^+CD11c^+$ cells. The expression of MHC II, CD86 and CD36 were analyzed in $CD11c^+$ DCs. (B) Representative flow cytometric plots show MHC II, CD86 and CD36 expression at Day 7. (C) The graphs show the expression of CD36, CD86 and MHC II in the BF and drLNs. N = 8 for Day 3, N = 14 for Day 7.

The expression of MHC II, CD86 and CD36 in monocytes/macrophages.

I also analyzed the expression of MHCII, CD86 and CD36 in monocytes/macrophages in the BF and drLNs. The gating strategy is shown in Fig. 6A. There were no statistically significant differences in the expression of the activation markers in both groups of the drLNs and BF (Fig. 6C). CD36 was expressed slightly higher in $CD11b^+$ cells in BF from allogeneic skin graft mice at Day 7, compared with the syngeneic ones ($p=0.06$) (Fig. 6C).

Figure 6.

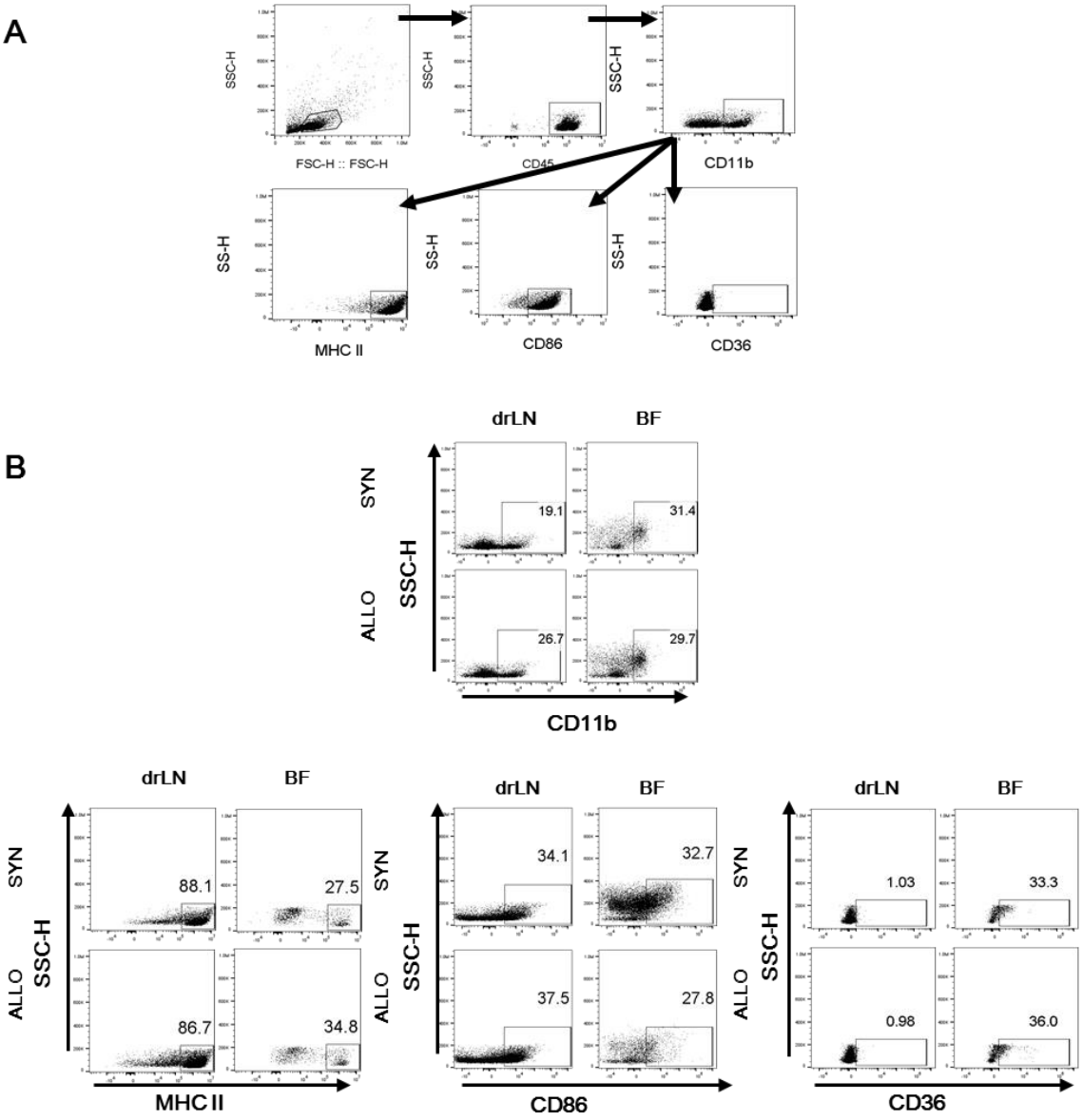
A
SSC-H
FSC-H :: FSC-H
CD45
CD11b
SS-H
MHC II
CD86
CD36
B
drLN
BF
SYN
ALLO
SSC-H
19.1
31.4
26.7
29.7
CD11b
88.1
27.5
86.7
34.8
MHC II
34.1
32.7
37.5
27.8
CD86
1.03
33.3
0.98
36.0
CD36

Figure 6. (continued)

C

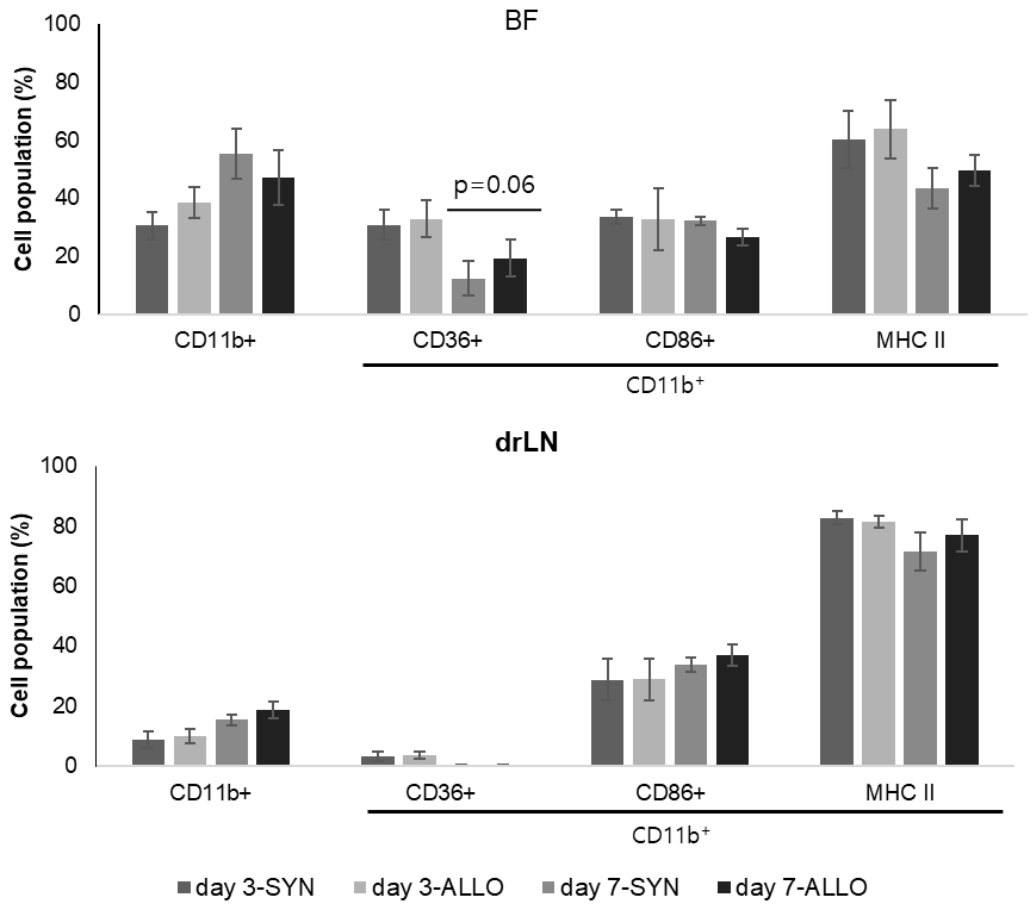

Figure 6. The expression of MHC II, CD86 and CD36 in monocytes/ macrophages cells

(A) Live cells were gated by SSC/FSC and immune cells were defined as $CD45^+$ cells. Monocytes/macrophages cells were defined as $CD45^+CD11b^+$ and the expression of MHC II, CD86 and CD36 were analyzed in $CD11b^+$ monocytes/macrophages. (B) Representative flow cytometric plots show the expression of MHC II, CD86 and CD36 from BF and drLNs at Day 7. (C) The graphs indicate the expression of CD36, CD86 and MHC II in the BF and drLNs. N = 8 for Day 3 and N = 14 for Day 7.

The expression of inflammatory monocytes in the BF in a skin graft model

$CD11c^{-}CD11b^{+}Ly6C^{hi}$ inflammatory monocytes, which traffic selectively to the sites of inflammation, produce inflammatory cytokines and contribute to local and systemic inflammation [43]. Hence, I evaluated their distribution in the BF and drLNs on Day 3 and Day 7 post skin graft (Fig. 7A). $CD11c^{-}CD11b^{+}Ly6C^{hi}$ inflammatory monocytes were more abundant in the BF, regardless of skin graft. They were slightly more in the BF and drLNs from allogeneic skin graft mice at Day 3 than syngeneic ones, but the differences were not statistically significant (Fig. 7B, C). The results suggest that inflammatory monocytes consist more in the BF than the secondary immune organs, regardless of stimulation.

Figure 7.

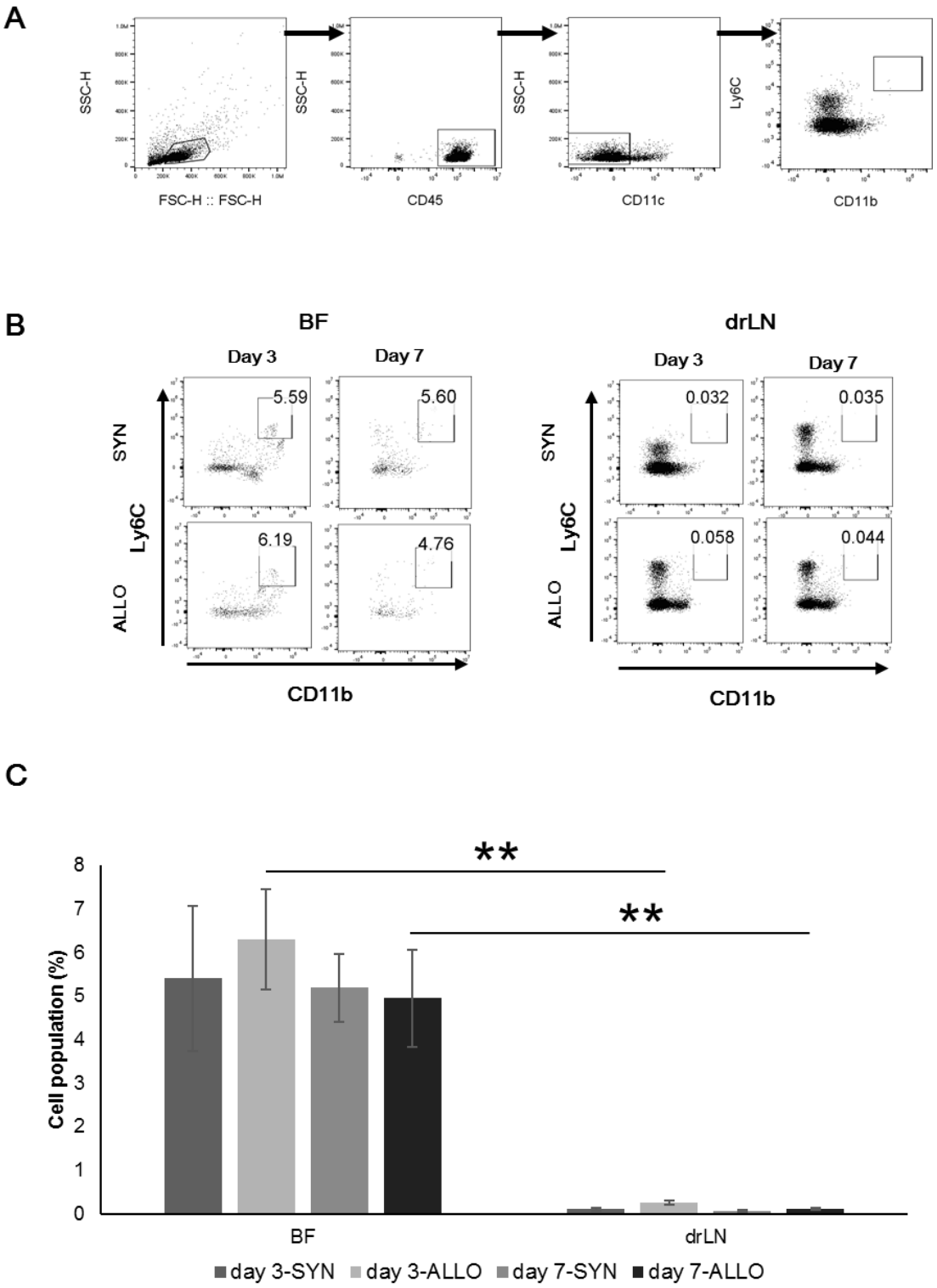
A
SSC-H
FSC-H :: FSC-H
SSC-H
CD45
SSC-H
CD11c
Ly6C
CD11b
B
BF
drLN
Day 3
Day 7
Day 3
Day 7
SYN
ALLO
Ly6C
5.59
5.60
6.19
4.76
0.032
0.035
0.058
0.044
CD11b
CD11b
C
**
**
Cell population (%)
8
7
6
5
4
3
2
1
0
BF
drLN
day 3-SYN
day 3-ALLO
day 7-SYN
day 7-ALLO

Figure 7. The expression of inflammatory monocytes in the BF in a skin graft model

(A) Live cells were gated by SSC/FSC and immune cells were defined as $CD45^{+}$. Inflammatory monocytes were defined as $CD11c^{-}CD11b^{+}Ly6C^{hi}$. (B) Representative flow cytometric plots show the inflammatory monocytes from the BF and drLNs at Day 3 and Day 7. (C) The graph displays the percentage of inflammatory monocytes in the BF and drLNs. N = 8 for Day 3, N = 14 for Day 7.

The expression of the enzymes in ceramide metabolism upon acute rejection

Lipid metabolism is central to the appropriate differentiation and functions of T lymphocytes. Ceramides are involved in sphingolipid metabolism, which plays a role in signaling pathways [44, 18, 19]. In particular, unpublished results of our lab showed the reduced a ceramide, C24, expression in the sera from the liver transplantation patients with rejection. Thus, I assessed the expression of the enzymes in ceramide metabolism in the liver by real-time Q-PCR as the liver is the main organ in lipid metabolism. Smpd1 and CerS5 expression were upregulated 1.4 folds and 1.8 folds, respectively, in the liver from allograft mice at Day 7 compared with syngeneic counterparts. This upregulation was of statistical significance (Fig. 8A). The results suggest that ceramide metabolism could play a role in the rejection.

Figure 8.

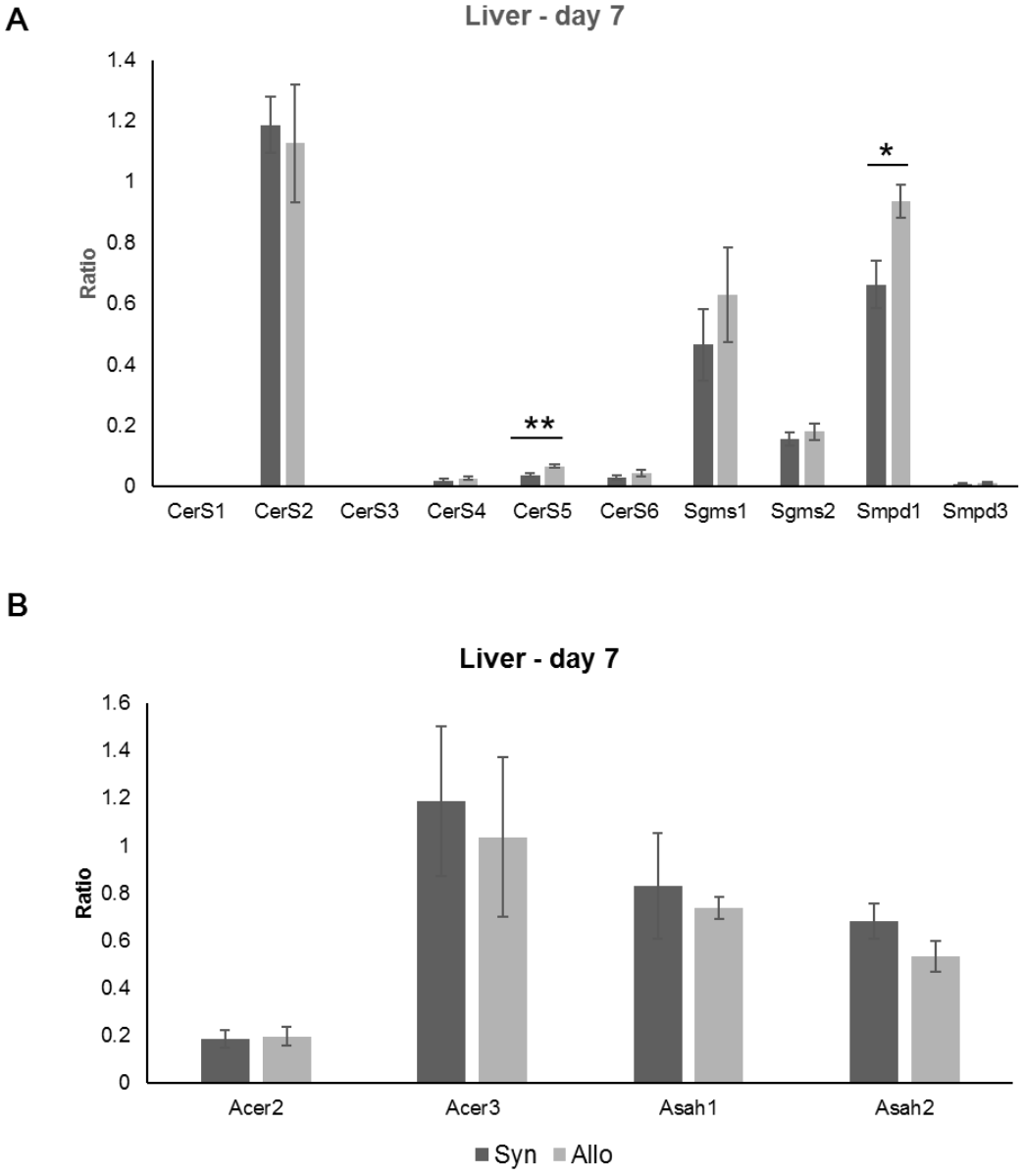
A
Liver - day 7
Ratio
1.4
1.2
1
0.8
0.6
0.4
0.2
0
**
*
CerS1
CerS2
CerS3
CerS4
CerS5
CerS6
Sgms1
Sgms2
Smpd1
Smpd3
B
Liver - day 7
Ratio
1.6
1.4
1.2
1
0.8
0.6
0.4
0.2
0
Acer2
Acer3
Asah1
Asah2
Syn
Allo

Figure 8. The expression of the enzymes in ceramide metabolism in the livers from skin graft mice

The mRNA expression of ceramide synthesis enzymes (A) and ceramidases (B) in the livers were analyzed by Q-PCR. The livers were harvested 7 days after skin graft. Each value was normalized to the expression of two house-keeping genes, which are *Gapdh* and *Hprt*. The data represents Mean + SEM. In case of CerS1-CerS6: N=8; Sgms1 and Sgms2: N=6; Spmd1 and Smpd3: N=4; Acer2-3 and Asah1-2, N=3.

Discussion

In this thesis, I demonstrate the roles of the BF resident-immune cells and that of ceramide metabolism in the liver in an allogeneic skin graft model. The immune cells in the BF displayed distinct characteristics in acute graft rejection. $CD8^+$ T cells and $CD36^+$ DCs in the BF might contribute to acute rejection.

Lymphocytes play vital roles in acute rejection [4]. After antigen stimulation, T cells can proliferate and differentiate into effector T cells [45]. $CD4^+$ T cells are stimulated by direct or indirect pathways, initiating the rejection process, and differentiate into effector T helper cells while $CD8^+$ T cells differentiate into cytotoxic T lymphocyte (CTLs) [45]. Memory $CD4^+$ T cells not only become effector cells upon reactivation but also provide help for the robust activation of donor-reactive effector $CD8^+$ T cells [46]. These effector $CD8^+$ T cells then are the main driving force behind allograft rejection and $CD8^+$ T cell depletion or limiting their trafficking into the graft significantly extends allograft survival [47, 46]. The phenotypes of immune cells in the drLNs in this research were similar to the results of Matesic D. *et al.* with a copious quantity of T cells responding to acute rejection [48]. The

lymphocyte number in the BF was not abundant, with low percentage of $CD4^+$ and $CD8^+$ T cells [48]. The percentages and absolute number of $CD8^+$ T cells were increased in the BF from allogeneic skin graft mice. Effector T cells in both $CD4^+$ and $CD8^+$ T cells expressed highly in the BF rather than in the drLNs. The BF in allograft mice contained similar numbers of immune cells to those in syngeneic ones, but the weight was reduced significantly. The density of immune cells in the BF from allograft mice was higher than the syngeneic counterparts in histology. The decreased weight of BF in allograft was not related to the change of immune cell number. The percentages of inflammatory monocytes in the BF were higher than those in the drLNs regardless of rejection. These results suggest that the BF responds in rejection by increasing effector lymphocytes. I also evaluated the expression of UCP1, a crucial protein for thermogenesis function of the BF, and there was no difference between syngeneic and allogeneic ones (data not shown).

After skin graft, T cells rapidly express CD69 upon stimulation by TCR hence it is known as the very early activation marker [49]. CD69 is also upregulated in T cells when exposed to type I IFN (IFNα/β) and other inflammatory mediators within the first hours of T

cells arriving in inflamed lymph nodes [50]. CD69 expressed in thymocytes following positive selection may ensure that T cells fully mature in the thymus prior to entering circulation [51]. In this study, the expression of CD69 was not different between allogeneic and syngeneic skin graft mice but higher at Day 7 than those at Day 3 in the drLNs. This phenomenon in the BF experienced only in $CD8^+$ T cells. It is supposed that more lymphocytes in the drLNs and $CD8^+$ T cell in the BF is activated and become mature in skin graft after 7 days. However, CD69 seems not to be a remarkable marker for allogeneic grafting.

In acute skin graft rejection, DCs and macrophages become mature and migrate to the lymph nodes then initiating an immune response by activating naive T cells [52]. DCs can be divided into two distinct subsets: conventional DCs (cDCs) and plasmacytoid DCs (pDCs) according to their immunophenotype and functional properties [53]. cDC1 have a superior ability to present antigens to $CD8^+$ T cells via MHC class I molecules, whereas cDC2 have a predominant role in MHCII-mediated antigens presentation to $CD4^+$ T cells [41]. pDCs are capable of promoting Treg expansion and function, as well as to suppress antigen-specific

immune responses both *in vitro* and *in vivo* [54]. Thus, pDCs incline to the tolerogenic effect on inducing donor T cells against host tissues [54]. In this research, $CD11c^+$ DCs were upregulated in the allograft, suggesting that more APCs migrated to the drLNs for mounting and activating T cells. However, this phenomenon was not seen in the BF. Although cDC2 expression in the drLNs was higher in allograft day 7 compared with the syngeneic counterpart, suggesting that more $CD4^+$ T cells would be activated to become effector lymphocytes. There was no difference in subsets of $CD4^+$ T cells in the drLNs. Both cDCs and pDCs expressed high in the BF, but the expression was not different between allogeneic and syngeneic skin graft mice. Hence, the APCs cells may not function in the BF in skin graft rejection.

Recognition of MHC class II by $CD4^+$ T cells stimulates their activation and differentiation into the subsets of T helper cells [55]. The efficient activation of naïve $CD4^+$ T cells requires a second signal to the lymphocyte in the form of co-stimulation to complete the APC-T cell interaction [56]. Classical costimulatory signals include CD80 and CD86 that interact with stimulatory CD28 [56]. Thus, I evaluated activation capacity by the

expression of CD86 and MHC II in DCs and macrophages. There was no difference in these markers between the syngeneic and allogeneic grafts in the drLNs and BF.

CD36 is a scavenger receptor that functions in high affinity tissue uptake of long-chain fatty acids and contributes under excessive fat supply to lipid accumulation and metabolic dysfunction [57]. CD36 is crucial for the function of monocytes/macrophages in glucose handling and lipid uptake to become foam cells in obesity and atherosclerosis [58]**.** CD36 expressed less in lymphocytes of the drLNs, while it showed higher expression in white adipose tissue and liver [59]. There was a borderline result about the expression of this marker in $CD4^+$ T cells between allograft and syngeneic graft. Meanwhile, both DCs and macrophages expressed high CD36 in allogeneic grafting, suggesting that this marker contributes to acute rejection. However, there may still be unknown the function of CD36 in lymphocytes in graft rejection. The underlying mechanism of CD36 in both $CD4^+$ T cells and APCs still awaits further investigation.

The expression of CerS5 and Smpd1 were upregulated in the liver upon acute rejection. The liver plays a key role in lipid metabolism, including sphingolipid metabolism

[60]. Ceramides are molecules of sphingolipid metabolism, which involved in cell proliferation, differentiation, inflammatory responses, and cellular apoptosis [18, 19]. The roles of sphingolipids in inflammation have been previously described [61, 62]. In addition, degradation of ceramides in the liver and adipose tissues results in improved glucose and lipid metabolism [63]. Our previous research showed a decrease in C24 ceramide in the sera in the acute skin graft model as well as in liver transplantation patients with acute rejection. Nonetheless, CerS5 and Smpd1 were expressed more in the liver from allogeneic skin graft mice. CerS5 is crucial for the synthesis of C16 ceramide, which is known as a pro-apoptotic factor [64, 65]. Both C16 ceramide and Smpd1 contribute to TNFα-induced hepatocyte apoptosis [65]. Hence, the liver or other affected organs may become inflammatory by increased apoptosis, responding to the allograft. However, both CerS5 and Smpd1 are not associated with the expression of C24 ceramide. Thus, the change of this ceramide in an allogeneic skin graft model still needs further investigation.

The current study is the first to document the role of immune cells in the BF and ceramide metabolism in acute skin graft rejection. The immune cells in the BF responded to

allogeneic skin graft by upregulating expression of $CD8^+$ T cells and effector T cell subsets in both types of lymphocytes, while APCs remained unchanged their expression. The activation markers for both lymphocytes and APC showed no difference between syngeneic and allogeneic skin graft. CD36 upregulation in APCs and $CD4^+$ T cells might result in the higher allogeneic immune responses in the BF. The expression of CerS5 and Smpd1 was increased in the liver in rejection. In conclusion, $CD8^+$ T lymphocytes and CD36 played roles in the BF to respond to the allogeneic skin graft rejection.

References

1. Gruskin, E. A., and R. Harten. 2016. 7 - Sourcing animal and human tissue for implant use. In *Extracellular Matrix-derived Implants in Clinical Medicine*. D. L. Mooradian, ed. Woodhead Publishing. 119-138.

2. Yang, J., J. C. Jeong, J. Lee, Y. H. Kim, H. C. Paik, J.-J. Kim, H.-Y. Park, M. S. Kim, and C. Ahn. 2017. Design and Methods of the Korean Organ Transplantation Registry. *Transplant Direct* 3: e191-e191.

3. VanBuskirk, A. M., W. J. Burlingham, E. Jankowska-Gan, T. Chin, S. Kusaka, F. Geissler, R. P. Pelletier, and C. G. Orosz. 2000. Human allograft acceptance is associated with immune regulation. *J Clin Invest* 106: 145-155.

4. Ingulli, E. 2010. Mechanism of cellular rejection in transplantation. *Pediatr Nephrol* 25: 61-74.

5. Marino, J., J. Paster, and G. Benichou. 2016. Allorecognition by T Lymphocytes and Allograft Rejection. *Frontiers in immunology* 7: 582-582.

6. Moreau, A., E. Varey, I. Anegon, and M.-C. Cuturi. 2013. Effector mechanisms of

rejection. *Cold Spring Harb Perspect Med* 3: a015461.

7. Howie, D., and C. Mauro. 2018. Editorial: Metabolism and Immune Tolerance. 9.

8. Ruiz, P., P. Maldonado, Y. Hidalgo, A. Gleisner, D. Sauma, C. Silva, J. J. Saez, Nu, #xf1, S. ez, M. Rosemblatt, and M. R. Bono. 2013. Transplant Tolerance: New Insights and Strategies for Long-Term Allograft Acceptance %J Clinical and Developmental Immunology. 2013: 15.

9. Sykes, M. 2007. Immune tolerance: mechanisms and application in clinical transplantation. 262: 288-310.

10. Lee, C.-F., Y.-C. Lo, C. Cheng, G. Furtmüller, B. Oh, V. Andrade-Oliveira, A. Thomas, C. Bowman, B. Slusher, M. Wolfgang, G. Brandacher, and J. Powell. 2015. Preventing Allograft Rejection by Targeting Immune Metabolism. *Cell reports* 13.

11. Shi, L. Z., R. Wang, G. Huang, P. Vogel, G. Neale, D. R. Green, and H. Chi. 2011. HIF1alpha-dependent glycolytic pathway orchestrates a metabolic checkpoint for the differentiation of TH17 and Treg cells. *J Exp Med* 208: 1367-1376.

12. Huynh, A., M. DuPage, B. Priyadharshini, P. T. Sage, J. Quiros, C. M. Borges, N.

Townamchai, V. A. Gerriets, J. C. Rathmell, A. H. Sharpe, J. A. Bluestone, and L. A. Turka. 2015. Control of PI(3) kinase in Treg cells maintains homeostasis and lineage stability. *Nature immunology* 16: 188-196.

13. Michalek, R. D., V. A. Gerriets, S. R. Jacobs, A. N. Macintyre, N. J. MacIver, E. F. Mason, S. A. Sullivan, A. G. Nichols, and J. C. Rathmell. 2011. Cutting edge: distinct glycolytic and lipid oxidative metabolic programs are essential for effector and regulatory CD4+ T cell subsets. *Journal of immunology (Baltimore, Md. : 1950)* 186: 3299-3303.

14. Howie, D., A. Ten Bokum, A. S. Necula, S. P. Cobbold, and H. Waldmann. 2018. The Role of Lipid Metabolism in T Lymphocyte Differentiation and Survival. 8.

15. Yin, Z., L. Bai, W. Li, T. Zeng, H. Tian, and J. Cui. 2019. Targeting T cell metabolism in the tumor microenvironment: an anti-cancer therapeutic strategy. *J Exp Clin Cancer Res* 38: 403-403.

16. O'Sullivan, D., G. J. van der Windt, S. C. Huang, J. D. Curtis, C. H. Chang, M. D. Buck, J. Qiu, A. M. Smith, W. Y. Lam, L. M. DiPlato, F. F. Hsu, M. J. Birnbaum, E. J.

Pearce, and E. L. Pearce. 2014. Memory CD8(+) T cells use cell-intrinsic lipolysis to support the metabolic programming necessary for development. *Immunity* 41: 75-88.

17. MacIver, N. J., R. D. Michalek, and J. C. Rathmell. 2013. Metabolic Regulation of T Lymphocytes. 31: 259-283.

18. Kurek, K., Wiesio, #x142, P. ek-Kurek, D. M. Piotrowska, #x141, B. ukaszuk, #x142, omiej, A. Chabowski, #x17b, M. endzian-Piotrowska, #x142, and gorzata. 2014. Inhibition of Ceramide De Novo Synthesis with Myriocin Affects Lipid Metabolism in the Liver of Rats with Streptozotocin-Induced Type 1 Diabetes %J BioMed Research International. 2014: 10.

19. Worgall, T. S. 2008. Regulation of lipid metabolism by sphingolipids. *Sub-cellular biochemistry* 49: 371-385.

20. Ballou, L. R., S. J. F. Laulederkind, E. F. Rosloniec, and R. Raghow. 1996. Ceramide signalling and the immune response. *Biochimica et Biophysica Acta (BBA) - Lipids and Lipid Metabolism* 1301: 273-287.

21. Herz, J., J. Pardo, H. Kashkar, M. Schramm, E. Kuzmenkina, E. Bos, K. Wiegmann,

R. Wallich, P. J. Peters, S. Herzig, E. Schmelzer, M. Kronke, M. M. Simon, and O. Utermohlen. 2009. Acid sphingomyelinase is a key regulator of cytotoxic granule secretion by primary T lymphocytes. *Nature immunology* 10: 761-768.

22. Taniguchi, M., H. Ogiso, T. Takeuchi, K. Kitatani, H. Umehara, and T. Okazaki. 2015. Lysosomal ceramide generated by acid sphingomyelinase triggers cytosolic cathepsin B-mediated degradation of X-linked inhibitor of apoptosis protein in natural killer/T lymphoma cell apoptosis. *Cell death & disease* 6: e1717-e1717.

23. Bai, A.-P., and Y. Guo. 2018. Ceramide is a Potential Activator of Immune Responses Against Tumors. *Gastroenterology* 155: 579-580.

24. Bai, A., E. Kokkotou, Y. Zheng, and S. C. Robson. 2015. Role of acid sphingomyelinase bioactivity in human CD4+ T-cell activation and immune responses. *Cell death & disease* 6: e1828.

25. Xu, J., B. A. Sayed, A. M. Casas-Ferreira, P. Srinivasan, N. Heaton, M. Rela, Y. Ma, S. Fuggle, C. Legido-Quigley, and W. Jassem. 2016. The Impact of Ischemia/Reperfusion Injury on Liver Allografts from Deceased after Cardiac Death

versus Deceased after Brain Death Donors. *PloS one* 11: e0148815-e0148815.

26. Carbone, F., C. La Rocca, P. De Candia, C. Procaccini, A. Colamatteo, T. Micillo, V. De Rosa, and G. Matarese. 2016. Metabolic control of immune tolerance in health and autoimmunity. *Seminars in immunology* 28: 491-504.

27. Huh, J. Y., Y. J. Park, M. Ham, and J. B. Kim. 2014. Crosstalk between adipocytes and immune cells in adipose tissue inflammation and metabolic dysregulation in obesity. *Molecules and cells* 37: 365-371.

28. Sethi, J. K., and A. J. Vidal-Puig. 2007. Thematic review series: adipocyte biology. Adipose tissue function and plasticity orchestrate nutritional adaptation. *J Lipid Res* 48: 1253-1262.

29. Rovira, J., M. Sabet-Baktach, E. Eggenhofer, M. Lantow, G. E. Koehl, H. J. Schlitt, J. M. Campistol, E. K. Geissler, and A. Kroemer. 2013. A color-coded reporter model to study the effect of immunosuppressants on CD8+ T-cell memory in antitumor and alloimmune responses. *Transplantation* 95: 54-62.

30. Čikoš, Š., A. Bukovská, and J. Koppel. 2007. Relative quantification of mRNA:

comparison of methods currently used for real-time PCR data analysis. *BMC Molecular Biology* 8: 113.

31. Uddin, M. M., I. Ohigashi, R. Motosugi, T. Nakayama, M. Sakata, J. Hamazaki, Y. Nishito, I. Rode, K. Tanaka, T. Takemoto, S. Murata, and Y. Takahama. 2017. Foxn1-β5t transcriptional axis controls CD8+ T-cell production in the thymus. *Nature Communications* 8: 14419.

32. Yuan, J., R. B. Crittenden, and T. P. Bender. 2010. c-Myb promotes the survival of CD4+CD8+ double-positive thymocytes through upregulation of Bcl-xL. *Journal of immunology (Baltimore, Md. : 1950)* 184: 2793-2804.

33. Schiffmann, S., K. Birod, J. Mannich, M. Eberle, M. S. Wegner, R. Wanger, D. Hartmann, N. Ferreiros, G. Geisslinger, and S. Grosch. 2013. Ceramide metabolism in mouse tissue. *The international journal of biochemistry & cell biology* 45: 1886-1894.

34. Peters, F., S. Vorhagen, S. Brodesser, K. Jakobshagen, J. C. Bruning, C. M. Niessen, and M. Kronke. 2015. Ceramide synthase 4 regulates stem cell homeostasis and hair

follicle cycling. *J Invest Dermatol* 135: 1501-1509.

35. Mitsutake, S., K. Zama, H. Yokota, T. Yoshida, M. Tanaka, M. Mitsui, M. Ikawa, M. Okabe, Y. Tanaka, T. Yamashita, H. Takemoto, T. Okazaki, K. Watanabe, and Y. Igarashi. 2011. Dynamic modification of sphingomyelin in lipid microdomains controls development of obesity, fatty liver, and type 2 diabetes. *J Biol Chem* 286: 28544-28555.

36. Lyn-Cook, L. E., Jr., M. Lawton, M. Tong, E. Silbermann, L. Longato, P. Jiao, P. Mark, J. R. Wands, H. Xu, and S. M. de la Monte. 2009. Hepatic ceramide may mediate brain insulin resistance and neurodegeneration in type 2 diabetes and non-alcoholic steatohepatitis. *J Alzheimers Dis* 16: 715-729.

37. Houston, D. A., K. Myers, V. E. MacRae, K. A. Staines, and C. Farquharson. 2016. The Expression of PHOSPHO1, nSMase2 and TNAP is Coordinately Regulated by Continuous PTH Exposure in Mineralising Osteoblast Cultures. *Calcified tissue international* 99: 510-524.

38. Lin, C. L., R. Xu, J. K. Yi, F. Li, J. Chen, E. C. Jones, J. B. Slutsky, L. Huang, B.

Rigas, J. Cao, X. Zhong, A. J. Snider, L. M. Obeid, Y. A. Hannun, and C. Mao. 2017. Alkaline Ceramidase 1 Protects Mice from Premature Hair Loss by Maintaining the Homeostasis of Hair Follicle Stem Cells. *Stem Cell Reports* 9: 1488-1500.

39. Avramopoulos, D., R. Wang, D. Valle, M. D. Fallin, and S. S. Bassett. 2007. A novel gene derived from a segmental duplication shows perturbed expression in Alzheimer's disease. *Neurogenetics* 8: 111-120.

40. Silaeva, Y. Y., A. A. Kalinina, L. M. Khromykh, and D. B. Kazansky. 2018. Functional properties of CD8+ T cells under lymphopenic conditions. *bioRxiv*: 353011.

41. Majdoubi, A., J. S. Lee, M. Balood, A. Sabourin, A. DeMontigny, O. A. Kishta, M. A. Moulefera, T. Galbas, T. J. Yun, S. Talbot, S. Ishido, C. Cheong, and J. Thibodeau. 2019. Downregulation of MHC Class II by Ubiquitination Is Required for the Migration of CD206(+) Dendritic Cells to Skin-Draining Lymph Nodes. *J Immunol* 203: 2887-2898.

42. Chistiakov, D. A., A. N. Orekhov, I. A. Sobenin, and Y. V. Bobryshev. 2014.

Plasmacytoid dendritic cells: development, functions, and role in atherosclerotic inflammation. *Front Physiol* 5: 279-279.

43. Kurihara, T., G. Warr, J. Loy, and R. Bravo. 1997. Defects in macrophage recruitment and host defense in mice lacking the CCR2 chemokine receptor. *J Exp Med* 186: 1757-1762.

44. Kitatani, K., J. Idkowiak-Baldys, J. Bielawski, T. A. Taha, R. W. Jenkins, C. E. Senkal, B. Ogretmen, L. M. Obeid, and Y. A. Hannun. 2006. Protein kinase C-induced activation of a ceramide/protein phosphatase 1 pathway leading to dephosphorylation of p38 MAPK. *J Biol Chem* 281: 36793-36802.

45. Wang, Q., and H. Wu. 2018. T Cells in Adipose Tissue: Critical Players in Immunometabolism. *Frontiers in immunology* 9: 2509-2509.

46. Chen, Y., P. S. Heeger, and A. Valujskikh. 2004. In vivo helper functions of alloreactive memory CD4+ T cells remain intact despite donor-specific transfusion and anti-CD40 ligand therapy. *Journal of immunology (Baltimore, Md. : 1950)* 172: 5456-5466.

47. Benichou, G., B. Gonzalez, J. Marino, K. Ayasoufi, and A. Valujskikh. 2017. Role of Memory T Cells in Allograft Rejection and Tolerance. *Frontiers in immunology* 8: 170-170.

48. Matesic, D., A. Valujskikh, E. Pearlman, A. W. Higgins, A. C. Gilliam, and P. S. Heeger. 1998. Type 2 Immune Deviation Has Differential Effects on Alloreactive CD4⁺and CD8⁺T Cells. *The Journal of Immunology* 161: 5236.

49. Ziegler, S. F., F. Ramsdell, and M. R. Alderson. 1994. The activation antigen CD69. *Stem cells (Dayton, Ohio)* 12: 456-465.

50. Grigorova, I. L., M. Panteleev, and J. G. Cyster. 2010. Lymph node cortical sinus organization and relationship to lymphocyte egress dynamics and antigen exposure. *Proc Natl Acad Sci U S A* 107: 20447-20452.

51. Cyster, J. G., and S. R. Schwab. 2012. Sphingosine-1-Phosphate and Lymphocyte Egress from Lymphoid Organs. 30: 69-94.

52. Goldstein, D. R., B. M. Tesar, S. Akira, and F. G. Lakkis. 2003. Critical role of the

Toll-like receptor signal adaptor protein MyD88 in acute allograft rejection. *J Clin Invest* 111: 1571-1578.

53. Koyama, M., D. Hashimoto, K. Aoyama, K.-i. Matsuoka, K. Karube, H. Niiro, M. Harada, M. Tanimoto, K. Akashi, and T. Teshima. 2009. Plasmacytoid dendritic cells prime alloreactive T cells to mediate graft-versus-host disease as antigen-presenting cells. *Blood* 113: 2088-2095.

54. Yu, H., Y. Tian, Y. Wang, S. Mineishi, and Y. Zhang. 2019. Dendritic Cell Regulation of Graft-Vs.-Host Disease: Immunostimulation and Tolerance. 10.

55. Roche, P. A., and K. Furuta. 2015. The ins and outs of MHC class II-mediated antigen processing and presentation. *Nat Rev Immunol* 15: 203-216.

56. Wosen, J. E., D. Mukhopadhyay, C. Macaubas, and E. D. Mellins. 2018. Epithelial MHC Class II Expression and Its Role in Antigen Presentation in the Gastrointestinal and Respiratory Tracts. 9.

57. Pepino, M. Y., O. Kuda, D. Samovski, and N. A. Abumrad. 2014. Structure-function of CD36 and importance of fatty acid signal transduction in fat metabolism. *Annu*

Rev Nutr 34: 281-303.

58. Kane, H., and L. Lynch. 2019. Innate Immune Control of Adipose Tissue Homeostasis. *Trends in immunology* 40: 857-872.

59. Couturier, J., A. M. Nuotio-Antar, N. Agarwal, G. K. Wilkerson, P. Saha, V. Kulkarni, S. K. Lakhashe, J. Esquivel, P. N. Nehete, R. M. Ruprecht, K. J. Sastry, J. M. Meyer, L. R. Hill, J. E. Lake, A. Balasubramanyam, and D. E. Lewis. 2019. Lymphocytes upregulate CD36 in adipose tissue and liver. *Adipocyte* 8: 154-163.

60. Nguyen, P., V. Leray, M. Diez, S. Serisier, J. Le Bloc'h, B. Siliart, and H. Dumon. 2008. Liver lipid metabolism. *Journal of animal physiology and animal nutrition* 92: 272-283.

61. Albeituni, S., and J. Stiban. 2019. Roles of Ceramides and Other Sphingolipids in Immune Cell Function and Inflammation. *Advances in experimental medicine and biology* 1161: 169-191.

62. Simon, J., A. Ouro, L. Ala-Ibanibo, N. Presa, T. C. Delgado, and M. L. Martínez-Chantar. 2019. Sphingolipids in Non-Alcoholic Fatty Liver Disease and

Hepatocellular Carcinoma: Ceramide Turnover. 21: 40.

63. Xia, J. Y., W. L. Holland, C. M. Kusminski, K. Sun, A. X. Sharma, M. J. Pearson, A. J. Sifuentes, J. G. McDonald, R. Gordillo, and P. E. Scherer. 2015. Targeted Induction of Ceramide Degradation Leads to Improved Systemic Metabolism and Reduced Hepatic Steatosis. *Cell metabolism* 22: 266-278.

64. Grosch, S., S. Schiffmann, and G. Geisslinger. 2012. Chain length-specific properties of ceramides. *Progress in lipid research* 51: 50-62.

65. Osawa, Y., H. Uchinami, J. Bielawski, R. Schwabe, Y. Hannun, and D. Brenner. 2005. Roles for C16-ceramide and Sphingosine 1-Phosphate in Regulating Hepatocyte Apoptosis in Response to Tumor Necrosis Factor. *The Journal of biological chemistry* 280: 27879-27887.

Abstract

Background: Graft rejection is a major drawback of allotransplantation in which T lymphocyte plays a vital role. Lipid metabolism is central to the appropriate differentiation and functions of T lymphocytes while adipose tissues are closely connected with the immune system. However, the characteristics and roles of immune cells are less investigated in the adipose tissues in rejection.

Purpose: This study is conducted to elucidate the immune responses in the brown fat in a murine skin graft model. The study could also help understand the role of ceramide metabolism in rejection.

Methods: Murine skin graft was performed on the left upper back of recipient mice by using allogeneic mouse tail skin. Mice were sacrificed after 3 or 7 days and immediately frozen in liquid nitrogen and then stored at -80˚C until use for Q-PCR to evaluate the expression of ceramide enzymes. Alternatively, fat tissues were fixed in Formalin for histology. Single cell

suspensions were prepared from the brown fats and draining lymph nodes and used for flow cytometry to analyze subsets of T lymphocytes and antigen-presenting cells.

Results: I found that there was a significant reduction of brown fat (BF) weight after skin allograft at Day 7, although there were no differences in the numbers of immune cells between syngeneic and allogeneic skin graft mice. The results of flow cytometry show that $CD8^+$ T cells and $CD36^+$ dendritic cells (DCs) were increased by allogeneic skin graft after 7 days, but there was no change in phenotypes of antigen-presenting cells (APCs). The expression of CerS5 and Smpd1 were upregulated in the liver by the allogeneic immune response at Day 7.

Conclusion: $CD8^+$ T cells and $CD36^+$ DCs in the BF may contribute to the acute rejection of skin graft. In addition, ceramide metabolism has changed by rejection. Suggesting that fat tissues and lipid metabolisms can be affected by rejection.